University of Bath

Alternative formats
If you require this document in an alternative format, please contact:
openaccess@bath.ac.uk

Hydrodynamic performance of a dual-floater hybrid system combining a floating breakwater and an oscillating-buoy type wave energy converter

Hengming Zhang[a], Binzhen Zhou [a, b*], Christopher Vogel[b], Richard Willden[b], Jun Zang[c**], Jing Geng[a]

[a]College of Shipbuilding Engineering, Harbin Engineering University, Harbin 150001, China
[b]Department of Engineering Science, University of Oxford, OX1 3PJ, United Kingdom
[c]Department of Architecture and Civil Engineering, University of Bath, Bath, BA2 7AY, UK

Abstract

The high cost of power generation impedes commercial-scale wave power operations. The objective of this work is to provide a cost-sharing solution by combining wave energy extraction and coastal protection. A two-dimensional numerical wave tank was developed using Star-CCM+ Computational Fluid Dynamics software to investigate the hydrodynamic performance of a dual-floater hybrid system consisting of a floating breakwater and an oscillating-buoy type wave energy converter (WEC), and was compared with published experimental results. The differences between the hydrodynamic performance of the hybrid system, a single WEC and a single breakwater were compared. Wave resonance in the WEC-breakwater gap has a significant impact on system performance, with the hybrid system demonstrating both better wave attenuation and wave energy extraction capabilities at low wave frequencies, i.e., wider effective frequency. Forces on the breakwater were generally reduced due to the WEC. Wave resonance in the narrow gap has an adverse effect on the energy efficiency of the hybrid system with an asymmetric WEC, while a beneficial effect with a symmetric WEC. The wave energy conversion efficiency of hybrid system can be improved by increasing the draft and width of the WEC and decreasing the distance between the WEC and the breakwater. The findings of this paper make wave energy economically competitive and commercial-scale wave power operations possible.

Key Word: Floating breakwater; Wave energy converter; Wave attenuation; Energy conversion efficiency; Wave resonance; Narrow gap

1. Introduction

The development of wave energy is constrained by high power generation costs, which are mainly due to the high cost of construction and low wave energy extraction performance of Wave Energy Converters (WECs) [1]. Integrating WECs with other marine structures may be an effective approach to reduce construction costs, improve wave extraction performance and achieve

---

cost-sharing, space-sharing, multi-functionality. This will make wave energy economically competitive, facilitating the development of floating breakwaters and WECs [2].

Proposed hybrid systems include Oscillating Water Column (OWC) WEC devices integrated with a breakwater and offshore wind turbines [3], overtopping type WEC integrated with a breakwater, and oscillating-buoy (OB) type WEC integrated with a floating breakwater. He et al. [4] studied experimentally the oscillating air-pressures inside the two chambers of an integrated OWC-type converter with a slack-moored floating breakwater, with the power extraction performance reported by He et al. [5]. The hydrodynamic performance of a pile-supported OWC breakwater was modeled analytically by He et al. [6] based on linear wave theory and matched eigenfunction expansion.

Xu et al. [7] experimentally studied the power extraction efficiency and hydrodynamic characteristics of a dual-functional device integrated OWC devices into a pile breakwater. Zheng et al. [8] developed a novel theoretical model based on the linear potential flow to study the performance of an OWC device integrated into a vertical structure. Giacomo et al. [9] investigated a WEC that combined a U-shape OWC and dielectric elastomer generator power take-off (PTO) through theoretical and experimental studies. Han et al. [10] numerically investigated the performance of a multi-level breakwater with an overtopping WEC consisting of two reservoirs with sloping walls at different levels. All of these studies showed that the power extraction and wave attenuation performance of the integrated OWC devices was improved.

The most widely studied floating breakwater and OB type WEC systems are the single-floater integrated system and the dual-floater hybrid system. The single-floater integrated system is comprised of a floating breakwater that also acts as the WEC with a power take-off (PTO) system, and has been studied theoretically, numerically and experimentally. Ning & Zhao [11] experimentally investigated the hydrodynamic performance of an OB type WEC integrated into a pile-restrained floating breakwater with rectangular cross-section, showing that the PTO damping force, wave height and draft of the floater significantly affected the performance of the integrated system. Similar conclusions were drawn by Zhao et al. [12], studying the same integrated system with linear potential flow theory. The predicted capture width ratio and heave RAO were much larger than the experimental results as the effect of viscosity was neglected. Computational Fluid Dynamics (CFD) methods have also been used as an approach that includes more physics than potential flow theory but is also cheaper than performing experiments. Chen & Zang [13] presented a hybrid numerical model based on the particle-in-cell method to study the wave attenuation and energy extraction performance of a WEC-type floating breakwater, which was experimentally studied by Ning & Zhao [11], and then further optimized the shape of this integrated system. The maximum energy efficiency of the single-floater integrated system was limited to the well-known maximum of 50% for heaving WECs with symmetric bottoms. However, the Berkeley Wedge, an

asymmetric heaving energy-capturing floating breakwater proposed by Yeung et al. [14], improved the energy-capturing efficiency to 96.34% at the resonant frequency and the transmission coefficient was also improved significantly [15], and the forces were obtained by computation using the Weakly Compressible Smoothed Particle Hydrodynamics (WCSPH) method and model-scale experiments [16].

Previous studies have showed that the performance of a single-floater integrated system is significantly affected by floater shape. Zhang et al. [17] investigated the hydrodynamic performance of four single-floater integrated systems with different bottom shapes, including square bottom, triangular bottom, Berkley Wedge bottom and novel triangular-baffle bottom. Floaters with an asymmetric bottom were found to have higher power conversion efficiency and better wave attenuation performance, especially for the Berkeley Wedge bottom and the triangular-baffle bottom. The geometry of the triangular-baffle bottom floater is simpler than the Berkeley Wedge yet it achieved similar wave attenuation and energy extraction characteristics, with maximum energy conversion efficiency of up to 93%. Additional adjustments to the device geometry were shown to further improve the energy conversion performance. However, in low frequency region, the wave attenuation and energy extraction performance of all four integrated systems were unsatisfactory, especially the system with square bottom.

The dual-floater hybrid system, consisting of a WEC and a floating breakwater behind the WEC, is an effective option to enhance the energy extraction and wave attenuation performance, particularly in the low frequency region. Ning et al. [18] developed an analytical model to investigate the hydrodynamics of a two-dimensional dual-pontoon floating breakwater that also worked as a WEC based on linear potential flow theory and matching Eigen-function expansion technique, showing a maximum conversion efficiency of this device up to 80%, although viscous effects were neglected. Zhao & Ning [19] experimentally investigated a two-pontoon system consisting of a front oscillating buoy type WEC and a rear fixed pontoon, revealing the wave energy extraction performance of the novel two-pontoon system was improved compared to the single pontoon system and the system with smaller draft ratio had better energy conversion performance. Zheng & Zhang [20] studied the performance of a hybrid WEC consisting of a fixed inverted flume and a long floating cube hinged with the flume, showing analytically that the power capture efficiency of the device for various geometrical parameters reached 95%. Reabroy et al. [21] investigated the hydrodynamic and power capture performance of an asymmetric WEC integrated with a fixed breakwater using Star-CCM+ software and experiment, and showed that the maximum power efficiency of the WEC was 0.376. Previous studies have focused on the hydrodynamic performance of hybrid systems with symmetric WECs, and have neglected wave resonance in the gap between the WEC and breakwater, which is one of the important differences between the

dual-floater hybrid system and the single-floater integrated system. Further, there has been little investigation to date on the performance of hybrid systems with asymmetric WECs.

Narrow gap wave resonance is a feature of dual-floater hybrid systems and has a significant impact on energy extraction performance. However, most research to date has studied the wave resonance in the narrow gap between two fixed bodies with symmetric bottoms, between a fixed box and a vertical wall, or between moving bodies without a PTO system, which are different to the case of dual-floater hybrid systems.

Li & Zhang [22] built a numerical wave tank based on fully-nonlinear potential-flow theory to study the effects of width and draft on wave resonance in the gap between two heaving barges. The results showed that the relative barge draft had a strong effect on resonance frequencies, and the relative breadth of the barges affected RAOs at resonance. Jiang et al. [23] numerically investigated 192 different cases of wave resonance between two side-by-side non-identical fixed boxes and found that the resonant frequency tended to reduce with increasing gap breadth, upstream and downstream box drafts, and that the incident wave steepness had very little effect on the resonant frequency. Ning et al. [24] studied the wave response in the gap between two barges using a time-domain potential-flow solver where the artificial viscosity coefficient was calibrated from physical experiments. The results indicated that the wave frequency corresponding to the largest wave amplitude in the gap decreased as barge draft increases, and the maximum wave height in the gap increased with the draft of the leeside barge, and decreased when incident waves propagated from larger draft barge to the smaller one. Feng et al. [25] presented a numerical study of the gap resonance between two side-by-side barges by using a multiphase Navier-Stokes equations model and showed that significant vortices were generated and shed from the sharp corners of the barges, and that the viscous damping associated with the twin-barge system was dependent on the incident wave steepness. Gao et al. [26] used OpenFOAM software to investigate the resonant water motion inside a narrow gap between two identical fixed boxes in a side-by-side configuration, analyzing the free-surface elevation in the narrow gap, wave loads on the bodies and the effects of the incident wave height on the reflection, transmission and energy loss coefficients.

It is not possible to infer the effect of wave resonance in the WEC-breakwater gap on the energy extraction performance of the dual-floater system from existing studies. The motivation and novelty of this work is twofold; firstly to investigate the effect of asymmetric WECs on the energy extraction and wave attenuation performance of a dual-floater hybrid system, and secondly to analyze the effect of wave resonance in the WEC-breakwater gap on the energy extraction of the WEC. This will help lead to cost-sharing WEC-breakwater solutions that help reduce the overall cost of wave energy.

The paper is structured as follows. In Section 2, the development of a two-dimensional numerical

wave tank by Star-CCM+ CFD software and each performance coefficient is defined. In Section 3, the convergence of the numerical model is studied and the proposed numerical wave tank is verified with published experimental results. In Section 4, the hydrodynamic performance of the dual-floater hybrid systems with symmetric and asymmetric WECs is studied and compared with their corresponding single-floater integrated system, and the effects of the wave resonance in the gap between a heaving WEC and a fixed breakwater on the hydrodynamic performance of the WECs are analyzed carefully. Then, the dual-floater hybrid system with asymmetric WEC is optimized in the terms of geometric parameters. Finally, the conclusions are presented in Section 5.

2. Numerical model

2.1 Numerical wave tank setup

A two-dimensional numerical wave tank was established using Star-CCM+ CFD software to simulate wave interaction with a hybrid system of a floating breakwater and an oscillating-buoy type WEC, as shown in Fig. 1. The WEC can only move in heave motion independently. The breakwater was assumed to be fixed because its motion was relatively small compared to the WEC. There was no coupling between the WEC and the breakwater, and the mooring system was not considered. The governing Navier-Stokes equations are spatially discretized using the finite volume method, and the Volume of Fluid (VOF) method is applied to capture the free surface interface between the air and water phases [27].
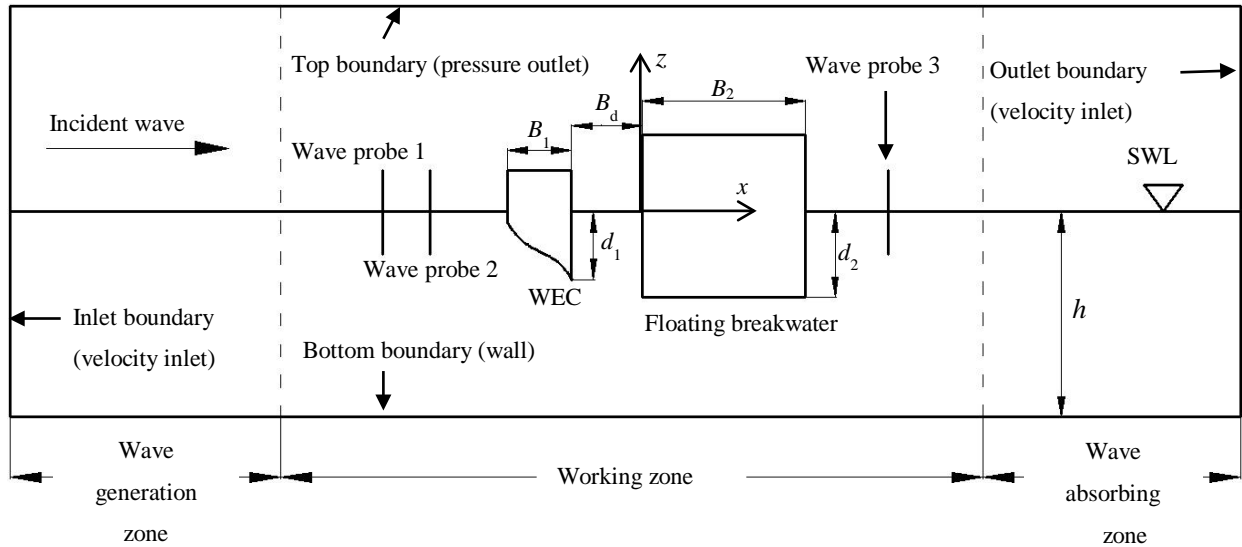

Fig. 1 A diagram of the two-dimensional numerical wave tank model

As shown in Fig. 1, the wave tank was divided into three zones: wave generation zone, working zone and wave absorbing zone. In this paper, the length of the numerical wave tank was six times the wavelength λ, which was verified in Section 3.1, and the height of the wave tank was two times the water depth h. The length of wave generation and damping zones were both 1.5λ. The VOF waves model included wave forcing [28] and wave damping [29] capabilities, which both can

reduce the computational domain size and thus reduce the disturbances by reflections from boundaries. The forcing method can be used at the inlet boundary to eliminate the reflecting waves before they reach the inlet boundary, while the damping approach cannot be applied at the inlet boundary to eliminate the effect of waves reflected by the body since the incoming waves would be damped as well. A previous study on these two wave absorbing methods demonstrated that the forcing method was better than the damping approach [17]. Therefore, the forcing method was applied in both wave generation and wave absorbing zones. The velocity inlet condition was assigned to both the inlet and outlet boundaries [17]. The inlet face velocity vector was specified as the velocity of a fifth-order VOF wave directly [30] and the working fluid was set to be two-phase flow of water and air. The top boundary was defined as a pressure outlet, where the pressure was specified as hydrostatic pressure of the fifth-order VOF wave [30] and the composition of fluid components was air. A no-slip wall boundary condition was assigned to the bottom of the domain. Since a purely two-dimensional planar model cannot be simulated with the Star-CCM+ software, the width of the model L_y in the y direction was set to 0.01m, which was verified in Zhang et al. [17], and symmetry conditions were applied to the lateral boundaries to ensure two-dimensionality [27][31].

Fig. 2 shows the mesh generation details of the wave tank model. A subtracted area was introduced when a floater was placed in the tank. No-slip boundary conditions were assigned to the body surface. The overset mesh condition was assigned to the outer four surfaces. A trimmed mesher model was used to generate the meshes of the liquid level encryption zone, the liquid surface transition zone and the motion encryption zone, as shown in Fig. 2. The Star CCM+ Trimmer generates hexahedral meshes that accommodate arbitrary geometry, and provides good quality meshes that have low computational cost. An overset mesh zone was applied in order to divide the complex air-water interface region into simpler sub-domains. The flow in each sub-domain was calculated independently, and may overlap with each other. Matching and coupling at the intersection of the two domains are performed by interpolation, which is based on the dynamic distinction of different cell types. The cells can be active (solve), inactive (ignore) or dependent (interpolate) [32]. The overset mesh approach has been used increasingly widely in CFD codes such as Star CCM+ and PEGASUS, because the meshing approach offers improved accuracy in comparison to dynamic meshes for large-scale deformations.
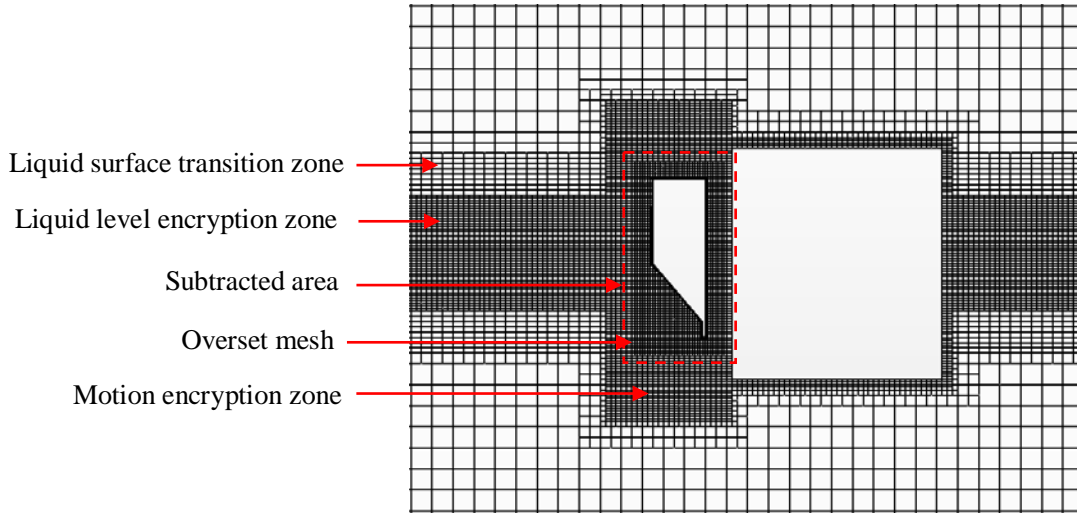
Fig. 2 Mesh generation details of the wave tank model

In our previous investigation [17], the experiment of a single-floater integrated system with box bottom by Ning & Zhao [11] and the experiment of a Berkeley Wedge floater by Madhi et al. [15] have been simulated using laminar flow model and large eddy simulation (LES) turbulence model, and the results of different turbulence models and laminar flow model were also compared. The preliminary study of higher-order turbulence models was not found to significantly affect floater motion when the width of the floater was relatively large [17]. The stability and accuracy of the wave tank using laminar flow model in generating waves has also been verified [17], with the maximum attenuation of wave heights being about 3.5% in the middle of the wave tank. As the focus of the present study is the motion of the floater, rather than the details of the flow field, the laminar flow model was selected.

2.2 Motion and energy conversion of floater

As there was no coupling between the WEC and the breakwater and the mooring system was not considered, the total forces on the WEC floater comprise the damping force and elastic stiffness force due to the power take-off (PTO) system, the gravity of the WEC floater, and the wave force. As the WEC was assumed to have heave motion only, the equation of motion is

$$m\ddot{z} + B_{pto}\dot{z} + c_{pto}z = -mg + F_w \tag{1}$$

where m is the mass of the floater; z, $\dot{z}$ and $\ddot{z}$ are the heave motion, velocity and acceleration of the floater, respectively; B_{pto} and c_{pto} are the mechanical damping and elastic stiffness due to the power take-off (PTO) system respectively, in which $c_{pto}=0$ is considered in present paper; F_w is the wave force, including buoyancy, in still water.

The resonance frequency is defined as [33]

$$\omega_{n} = \sqrt{\frac{c_{pto} + c_{z}}{m + a_{z}}} \tag{2}$$

For a single body with only a single mode of motion, the optimal damping coefficient B_{opt} under wave frequency ω can be written as [33]

$$B_{opt} = \sqrt{\frac{((m + a_{z})\omega^2 - (c_{pto} + c_{z}))^2}{\omega^2} + b_{z}^2} \tag{3}$$

where a_{z} and b_{z} are the linear added mass and radiation damping coefficients of the floater, which are both functions of wave frequency and calculated through a two-dimensional numerical wave tank model based on potential flow theory [34][35]. $c_{z} = \rho g A_{w}$ is the restoring force coefficient due to the difference in the contributions from the hydrostatic term and the weight of the floater, in which A_{w} is the wetted surface of the floater.

The energy conversion efficiency η_{e} is an important indicator of the hydrodynamic efficiency of WECs [36], which can be expressed as

$$\eta_{e} = E_{p} / E_{w} \tag{4}$$

where the average wave energy conversion power and the incident wave power are calculated as:

$$E_{P} = \frac{B_{pto}}{nT} \int_{t}^{t+nT} V^2 \mathrm{d}t \tag{5}$$

$$E_{w} = \frac{1}{16} \frac{\rho g H_{i}^{2} \omega D_{y}}{k} (1 + \frac{2kh}{\sinh 2kh}) \tag{6}$$

where H_{i} is the incident wave height, h is the water depth, V is the velocity of the floater, T is the wave period, D_{y} is the transverse length of floating breakwater, and n is the number of the floater motion period.

Two wave probes were placed at $x_{1} = -1.6$m and $x_{2} = -1.0$m in front of the WEC to separate the incident wave height H_{i} and reflection wave height H_{r} by using two-point method, and another one was placed at $x_{3} = 0.8$m behind the breakwater to measure the transmission wave height H_{t}, as shown Fig. 1. The reflection coefficient K_{r} is defined as $K_{r} = H_{r}/H_{i}$, and the wave transmission coefficient which is an important consideration of the wave protection role of a breakwater is defined as $K_{t} = H_{t}/H_{i}$. The accuracy of wave probe placement was validated by comparing the reflection coefficient and transmission coefficient of CFD results with those of experimental results by Zhao & Ning [19] in Section 3.2. The dissipative wave energy, such as the wasted energy by vortex shedding at the edge of floaters, is measured by dissipation coefficient K_{d}, which is defined as

$$K_{d} = 1 - K_{t}^{2} - K_{r}^{2} - \eta_{e} \tag{7}$$

The motion response ζ is defined as $\zeta = H_{RAO}/ H_{i}$, where H_{RAO} is floater motion amplitude .

3. Convergence study and verification
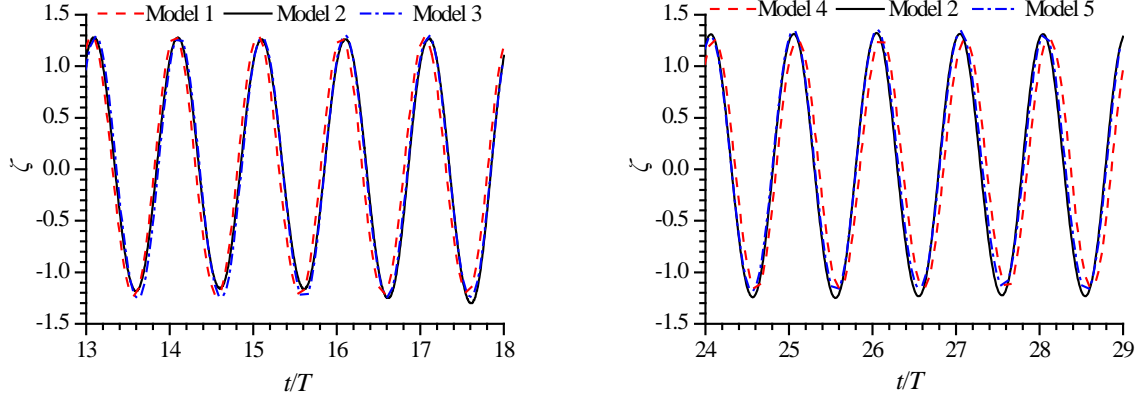
3.1 Convergence study

A hybrid system of a fixed breakwater and a WEC with triangular-baffle, a representative case of the present paper, was chosen to carry out the mesh and time convergence studies. The width of the triangular-baffle floater was $B_1/h=0.167$ and the draft was $d_1/h=0.267$, where the water depth $h=3.0$m. The width and the draft of the breakwater were $B_2/h=0.667$ and $d_2/h=0.4$, the incident wave height $H_i/h=0.1667$ and the distance between WEC and breakwater $B_d/h=0.0833$. Five models with different meshes and different time steps (denoted Models 1-5) were investigated under the optimal PTO damping $b_{opt}=4.5$kg/s at $\omega=4.06$rad/s. Details of the meshes and time steps for the convergence study with $H_i=0.5$m at $T=1.72$s are shown in Table 1.

Fig. 3 compares the heave motion of the triangular-baffle floater with different meshes and time steps. Fig. 3(a) shows that Model 1 does not match well with Model 2 and Model 3 with the phase difference greater than 5%, and an amplitude difference of less than 5%. Only slight differences are observed between Model 2 and Model 3. Only slight differences between Models 2 and 5 are observed in Fig. 3 (b), less than 5% in peaks and troughs, whereas a phase shift $\Delta(t/T)$ greater than 0.07 when $t/T>24$ and an amplitude difference of almost 6% is observed for Model 4. It was concluded that Model 2 with mesh $\Delta z=H/20$, $\Delta x=2\Delta z$ and time step $\Delta t=T/1000$ is sufficiently converged. Therefore, the Model 2 is applied in following cases.

Fig. 4 shows the comparison of heave motion ζ of a triangular-baffle bottom WEC of the hybrid system with different lengths of tank, where the wave height $H_i/h=0.167$, the wave period $T=1.72$s. A significant phase difference $\Delta(t/T)>0.03$ develops for $t/T>13$ when $L_x=4\lambda$ in comparison to $L_x=6\lambda$ and $L_x=9\lambda$. The amplitude difference is around 6.6%, while only slight difference exists between the results of $L_x=6\lambda$ and $L_x=9\lambda$ in peaks and troughs, less than 6.25%. Therefore, $L_x=6\lambda$ is considered to be long enough to simulate this case.

Table 1 Time step and mesh size details of a hybrid system model consisting of a fixed breakwater and a WEC with triangular-baffle for convergence study with $H_i=0.5$m at $T=1.72$s

Models	Time steps	Meshes
1	$\Delta t=T/500$	$\Delta z=H_i/20$, $\Delta x=H_i/10$
2	$\Delta t=T/1000$	$\Delta z=H_i/20$, $\Delta x=H_i/10$
3	$\Delta t=T/2000$	$\Delta z=H_i/20$, $\Delta x=H_i/10$
4	$\Delta t=T/1000$	$\Delta z=H_i/10$, $\Delta x=H_i/5$
5	$\Delta t=T/1000$	$\Delta z=H_i/40$, $\Delta x=H_i/20$

(a) Convergence study with time step   (b) Convergence study with mesh resolution

Fig. 3 Convergence study with (a) time step and (b) mesh resolution for heave motion of a triangular-baffle bottom WEC of the hybrid system with H_i=0.5m at T=1.72s
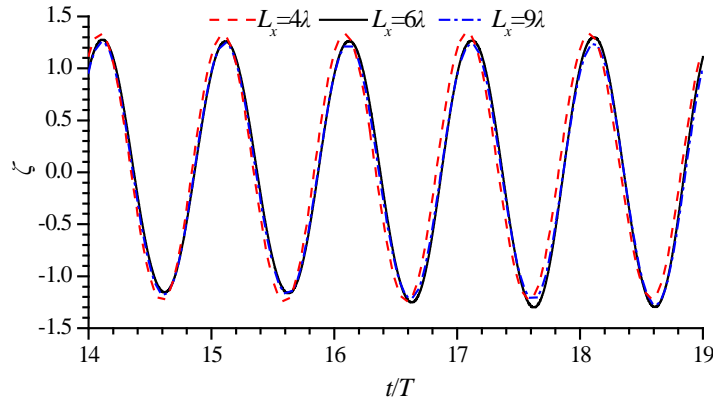

Fig. 4 Convergence study of tank length L_x for heave motion of a triangular-baffle bottom WEC of the hybrid system with H_i=0.5m at T=1.72s

### 3.2 Comparison of published experimental and numerical results

To validate the present CFD model, the experiment of a breakwater-type WEC composed of two floating pontoons with square bottom by Zhao & Ning [19] was simulated, with drafts $d_1=d_2$=0.125m, breadths $a_1=a_2$=0.6m and the distance between pontoons s=0.2m. The front pontoon moved only in heave mode, and the rear one was fixed. The still water depth was 1.0m. Table 2 shows the test conditions for the dual-pontoon system, including the PTO damping forces F_{pto} non-dimensionalized by $\rho g a_1 d_1 D_1$ (in which D_1=0.78m is the transversal length of pontoon), related wave perids T and wave amplitude A. Fig. 5 compares the present CFD results using the laminar flow model and the experimental results by Zhao & Ning [19], which show similar trends. The additional damping forces due to factors such as the friction between floater and vertical pile, result in a small difference between the CFD results and experiment results, especially for the conversion efficiency η_e and the heave motion ζ. Nevertheless, the overall agreement between CFD results and experiment results is sufficient for the purposes of understanding the wave transmission and energy conversion trends of hybrid WEC-breakwater systems in this paper.

Table 2 Test conditions for the dual-pontoon system by Zhao & Ning [19] with $a_1=a_2$=0.6m, $d_1=d_2$=0.125m.

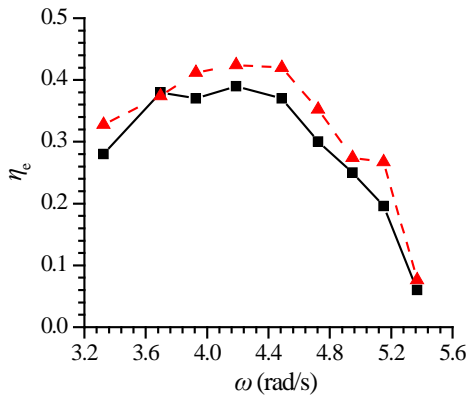| T (s)	1.17	1.22	1.27	1.33	1.4	1.5	1.6	1.7	1.89
ω (rad/s)	5.37	5.15	4.95	4.72	4.49	4.19	3.93	3.69	3.24
A (m)	0.04	0.06	0.06	0.07	0.07	0.07	0.07	0.07	0.07
F_{pto}	0.0169	0.0563	0.0679	0.0854	0.1036	0.0981	0.1017	0.1003	0.104
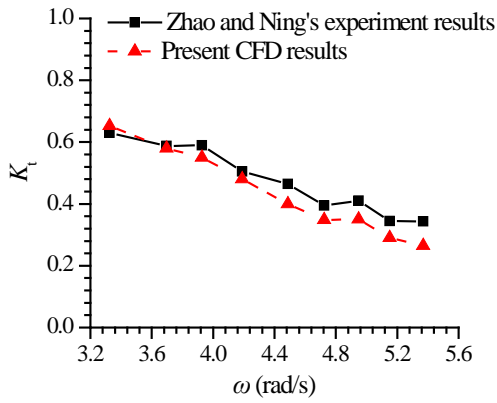
(a) Transmission coefficient
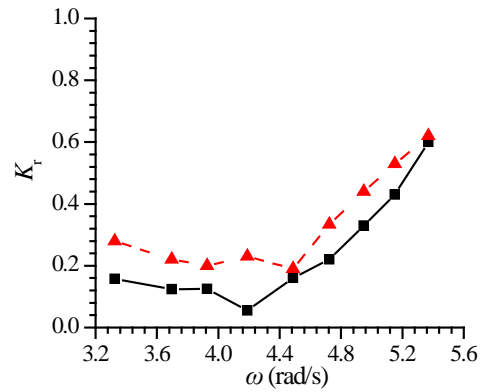
(b) Reflection coefficient

(c) Conversion efficiency
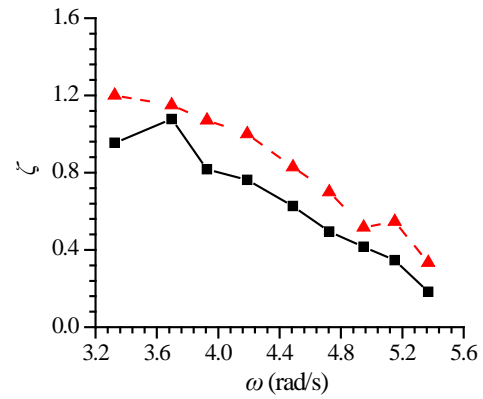
(d) Heave motion
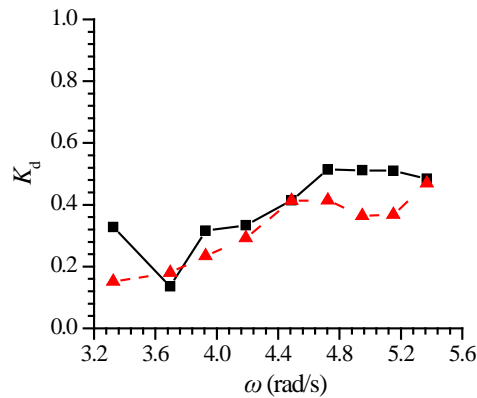
(e) Dissipation coefficient

Fig. 5 Comparison of the present CFD results and the experimental results by Zhao & Ning [19]

3.3 Verification of optimal PTO damping

The optimal PTO damping coefficient B_{opt} used in the following investigation was obtained by Eq. (3), based on potential flow theory. To verify the accuracy of Eq. (3), a hybrid system CFD model consisting of a square bottom WEC and a stationary floating breakwater was established. The draft and width of WEC were $d_1/h=0.131$ and $b_1/h=0.233$, respectively. The draft of the floating breakwater was $d_2/h=0.4$, and the width of the floating breakwater was $B_2/h=0.667$. The still water depth was $h=3$m and the incident wave height was $H_i=0.5$m. The wave periods and relative PTO damping coefficients B_{pto} for a hybrid system model consisting of a square bottom WEC and a stationary floating breakwater are summarised in Table 3. Fig. 6 shows the variations of energy conversion efficiency η_e versus PTO damping coefficient of the hybrid system CFD model at three different wave periods. For the three wave periods the energy conversion efficiency η_e of WEC is maximised when $B_{pto}/B_{opt}=1$, illustrating that potential flow theory provides an accurate method for determining the optimal damping B_{opt}. In the following cases, the optimal damping coefficients for each case were obtained using Eq. (3) to maximising conversion efficiency.

Table 3 Details of wave periods and relative PTO damping coefficients for a hybrid system model consisting of a square bottom WEC and a stationary floating breakwater

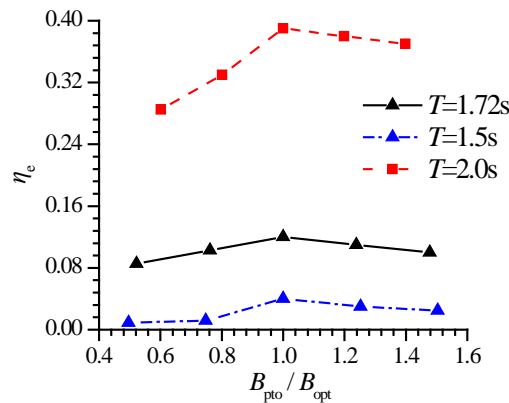| Wave periods (s)	B_{opt} (kg/s)	B_{pto} (kg/s)
1.5	7.94	3.94, 5.94, 7.94, 9.94, 11.94
1.72	8.38	4.83, 6.83, 8.83, 10.83, 12.83
2.0	10.05	6.05, 8.05, 10.05, 12.05, 14.05

Fig. 6 Variations of η_e versus PTO damping coefficient of a hybrid system CFD model consisting of a square bottom WEC and a stationary floating breakwater with $H_i=0.5$m at three different wave periods

## 4. Performance study of the hybrid system

4.1 Comparison of single and dual floaters

To investigate the interactions between the WEC and breakwater, three different models were

considered: a single breakwater, a single WEC, and the combined breakwater-WEC system. It was previously shown that an asymmetric floater (triangular-baffle bottom) has higher power conversion efficiency and better wave attenuation performance than a symmetric one with square bottom in the absence of a breakwater [17]. However, the presence of the breakwater may affect the performance of a WEC in an integrated system due to wave reflection from the breakwater. Therefore, WECs with triangular-baffle and square bottoms were both considered in this study. The water depth was $h=3.0$m, and the normalized incident wave height was $H_i/h=0.167$. The distance between the WEC and the breakwater was $B_d/h=0.083$ and the displacement of both WECs was $V=0.275$m^3. Other parameters are detailed in Fig. 7. The parameters of the WECs followed that of previous investigations of the single-floater integrated system [17]. Representative dimensions for the breakwater were assumed. From Section 4.2 to 4.4, the choice of parameter values follows previous studies, such as the studies of Zhang et al. [17], Zhao & Ning [19] and Jiang et al. [23].
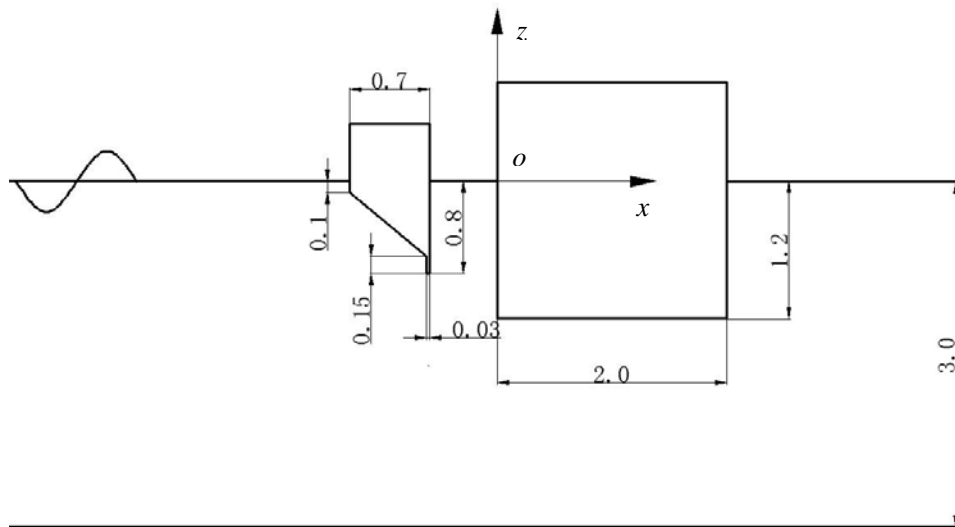
(a) Triangular-baffle bottom WEC
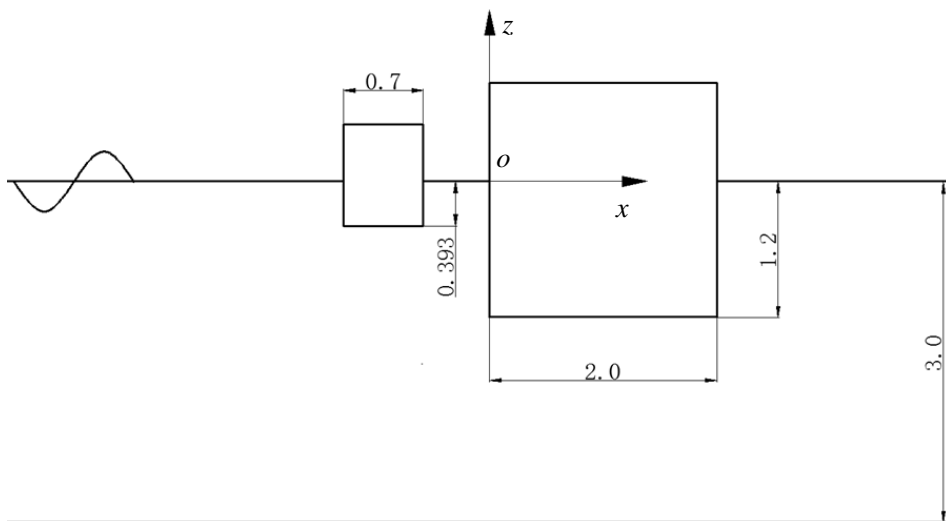
(b) Square bottom WEC

Fig. 7 Schematic diagrams of a) triangular-baffle and b) square bottom WECs integrated with a box-type

breakwater (units: m)

The variation of the transmission coefficient K_t, reflection coefficient K_r, conversion efficiency η_e, heave motion ζ, dissipation coefficient K_d and wave response in the middle of gap H/H_i with wave frequency for the three models are shown in Fig. 8 for the triangular-baffle WEC and Fig. 9 for the square WEC. Fig. 8 (a) and Fig. 9 (a) show that K_t decreases in all cases with increasing wave frequency, implying that the wave attenuation performance of floaters is better for short rather than long waves. K_t for the hybrid system is generally the lowest among three models. K_t is greatly reduced compared with the WEC-only cases, with a maximum reduction ratio of 86.3% for the triangular-baffle and 92.6% for the square hybrid WEC-breakwater systems respectively, both at ω=3.65rad/s. There is little difference between K_t for the breakwater and hybrid systems because the draft of breakwater is significantly larger than that of the WEC, which is the main factor for the transmission coefficient.

The reflection coefficient K_r of the hybrid system is generally less than that of the breakwater but larger than that of the single WEC in lower frequencies, as seen in Fig. 8 (b) and Fig. 9 (b), particularly near the resonance frequency (ω_n=3.65rad/s). At higher frequencies the differences in K_r of the three models reduces. Deploying a WEC in front of the breakwater results in absorption of energy that reduces K_r, which is particularly significant at frequencies close to that for peak conversion efficiency. This effect is especially important for the asymmetric triangular-baffle WEC which is capable of achieving a higher conversion efficiency than the symmetric square WEC.

Fig. 8(f) and Fig. 9 (f) show there is wave resonance in the gap near ω=2.79rad/s for the triangular-baffle hybrid system and ω=2.62rad/s for the square one, similar to the findings of Jiang et at. [23]. The wave elevation in the WEC-breakwater gap of the hybrid system with triangular-baffle WEC is larger than that for a single breakwater around the wave resonance frequency ($3.14<\omega<3.8$rad/s). The opposite occurs for the hybrid system with square WEC, as shown in Fig. 9(f). At higher frequencies, the wave elevations in the WEC-breakwater gap of the hybrid systems are smaller than that of a single breakwater measured at the same position. The wave elevations in the middle of WEC-breakwater gap are larger than that of the single WEC for all frequencies. The dissipation definition in Eq. (7) includes contributions from the energy losses due to vortex shedding at the edge of floaters and the energy in the gap region for the hybrid system. Therefore, wave resonance in the gap leads to the increased dissipation coefficient and reduction in heave motion and conversion efficiency in Fig. 8.

Fig. 8 (c) and Fig. 9 (c) show that the conversion efficiency η_e of the hybrid system increases substantially in the low frequency region for both the symmetric and asymmetric WEC designs compared with the single WEC. The maximum η_e of the square bottom WEC in the hybrid system is greatly improved compared with the single WEC, by up to 2.24 times, with a significant change

14

in the peak frequency (ω_n=2.62rad/s) compared to the single WEC (ω_n=3.65rad/s). It is notable that this is higher than the theoretical maximum energy-capture efficiency of 50% for a symmetric heaving device. There is almost no change in peak η_e for the asymmetric triangular baffle WEC when deployed in the hybrid system, in both cases reaching η_e=0.72. A portion of the waves transmitted by the WEC are then reflected by the breakwater back towards the WEC, particularly at low frequency. The lower draft of the square WEC compared to the triangular-baffle WEC means that more waves are transmitted past the WEC and then reflected by the breakwater. Consequently, the WECs in the hybrid system are also able to extract energy from waves reflected from the breakwater, as seen in the heave motion shown in Fig. 8(d) and Fig. 9 (d), boosting overall conversion efficiency in comparison to the standalone WEC cases. This effect is particularly significant for the square WEC as its symmetry means that the hydrodynamics of energy conversion is the same for both directions of wave propagation. The asymmetric triangular-baffle WEC does not have the same η_e for waves propagating in the forwards and backwards directions. η_e is very low for waves propagating in the backwards direction, and hence the triangular-baffle WEC has relatively less benefit from the presence of the breakwater.

Wave reflection from the breakwater in the hybrid system also results in larger wave resonance in the middle of the WEC-breakwater gap than those in the equivalent position behind the single WEC in the low frequency region ω<3.80rad/s, especially at ω=2.62rad/s, where the maximum wave elevations occurs, i.e., waves resonant in the gap. Therefore, the heave motion ζ in Fig. 9 (d) and the conversion efficiency η_e in Fig. 9 (c) are improved greatly near ω=2.62rad/s.

It can be seen from Fig. 8 (e) and Fig. 9 (e) that the dissipation coefficient K_d for the single WEC is smallest around the resonance frequency (3.14<ω<3.8rad/s) because most of the available energy is absorbed by the PTO system. It can also be seen that the smallest K_d of the hybrid system appears at the lower frequency mainly because the transmission and reflection coefficients at lower frequency are much larger than other frequencies. Since the ratio of the size of the floater to wave length becomes larger as wave frequency increases, viscous effects increase, leading to greater energy dissipation and thus larger K_d.
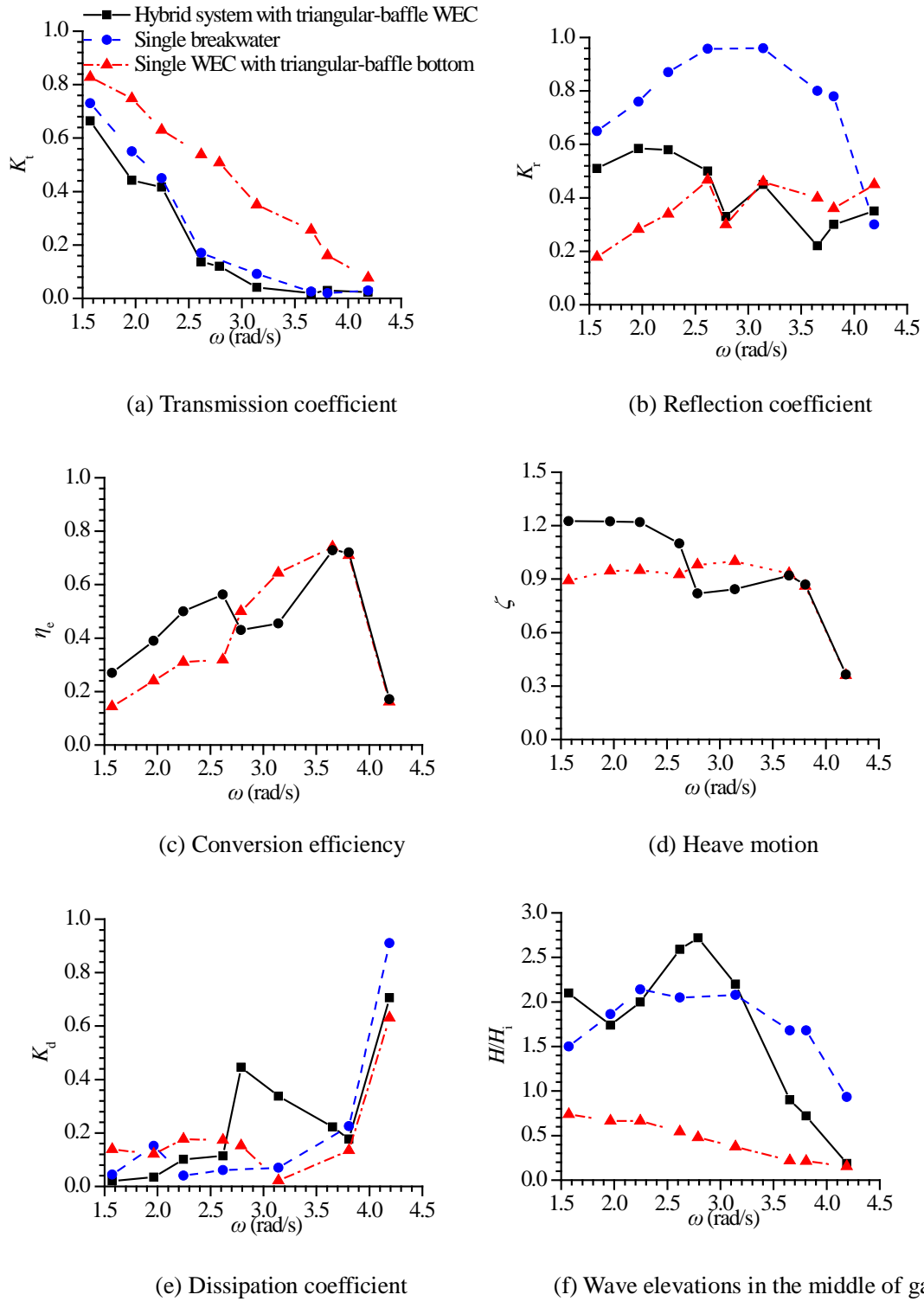
(a) Transmission coefficient

(b) Reflection coefficient

(c) Conversion efficiency

(d) Heave motion

(e) Dissipation coefficient

(f) Wave elevations in the middle of gap

Fig. 8 Variations of K_t, K_r, η_e, ζ, K_d and H/H_i versus ω for different models with the triangular-baffle WEC under the optimal PTO damping

(a) Transmission coefficient

(b) Reflection coefficient

(c) Conversion efficiency

(d) Heave motion

(e) Dissipation coefficient

(f) Wave elevations in the middle of gap
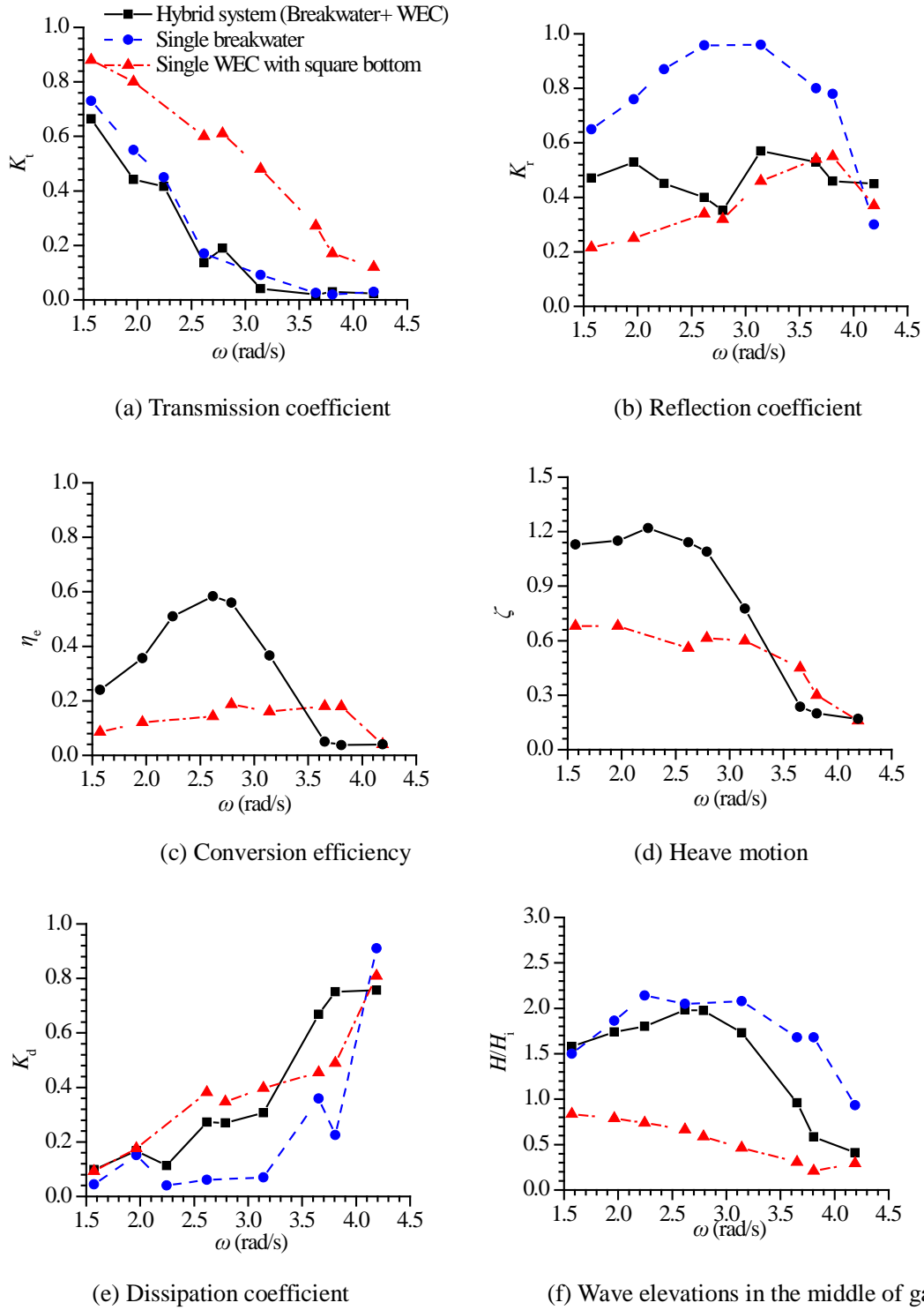
Fig. 9 Variations of K_t, K_r, η_e, ζ, K_d and H/H_i versus ω for different models with the square-bottom WEC under the optimal PTO damping

Fig. 10 shows the ratio of vertical and horizontal force on the breakwater for the hybrid system with triangular-baffle bottom and square bottom WECs to that for the single breakwater. Deploying a WEC in front of the breakwater generally reduces the vertical and horizontal forces on the breakwater, especially near the resonance frequency where the WEC removes the most energy from

17

the wave. The maximum reduction ratios for the breakwater with triangular-baffle WEC, relative to the single breakwater, are about 70.0% for the vertical force at ω=4.19 rad/s and 80.0% for the horizontal force at ω=3.8 rad/s, respectively. For the breakwater with square WEC, these ratios are 66.7% at ω=3.8 rad/s for the vertical force and 70.7% at ω=4.19 rad/s for the horizontal force, respectively. The forces on the breakwater are directly related to the wave elevation in front of breakwater because the transmitted waves behind it are relatively much smaller. Fig. 9 (f) shows the wave elevation of the hybrid system in the gap with square WEC in front of breakwater is generally smaller than that of the single breakwater, resulting in the horizontal and vertical forces on the breakwater become smaller. However, the wave elevation of the hybrid system in the gap with triangular-baffle WEC in Fig. 8 (f) is larger than that of the single breakwater near the resonant frequency, leading to the increase of the forces. Although the triangular-baffle WEC captures higher energy than the square WEC, the reduction in force on the breakwater is greater for the hybrid system with square WEC when 2.0<ω<3.65 rad/s.

(a) Vertical force   (b) Horizontal force
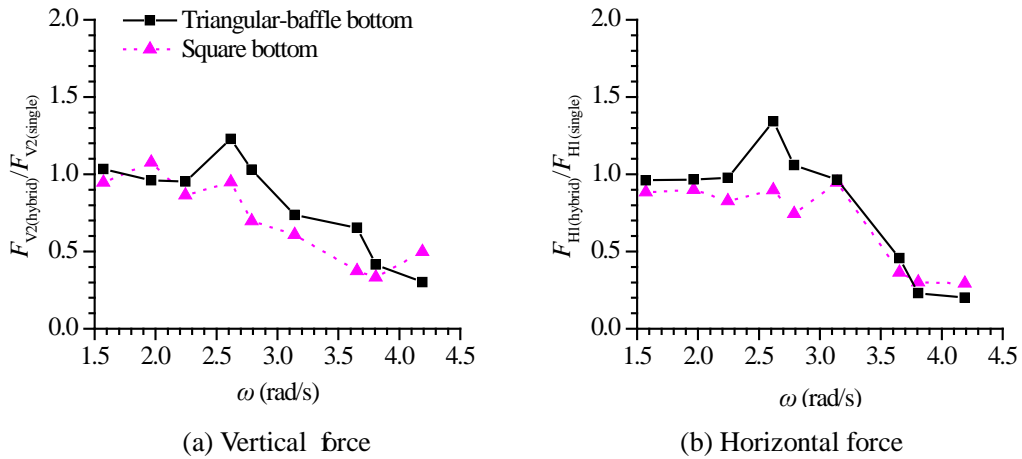
Fig. 10 Comparison of vertical and horizontal forces on the single breakwater and the breakwaters of the hybrid system with triangular-baffle and square bottom WEC under the optimal PTO damping

4.2 Effect of distance between WEC and breakwater

The effect of the distance between the WEC and breakwater was investigated for the hybrid breakwater and triangular-baffle WEC system at three different distances of B_d/h=0.0833, 0.167 and 0.333. All other dimensions remained unchanged. Fig. 11 shows the variation of transmission coefficient K_t, reflection coefficient K_r, conversion efficiency η_e, dissipation coefficient K_d, heave motion ζ and wave elevation in the middle of gap H/H_i of the hybrid system against wave frequency for different distances.

The transmission coefficient K_t is largely unaffected by the distance B_d, as K_t is primarily a function of the draft. K_r is minimum for all designs at ω=3.65 rad/s, where conversion efficiency η_e is maximised in all cases. Conversion efficiency η_e reduces more quickly as the distance increases

as the wave frequency moves away from the resonance frequency, i.e. the effective frequency width is larger for the smaller distance. Jiang et al. [23] found that the resonant frequency tended to be smaller as the gap width increases, but the variation trend of wave resonance in the gap was not regular. Fig. 11 (f) also show that the resonant frequency and the wave resonance in the gap decrease as the gap width increases. The corresponding resonant frequencies are ω=3.14 rad/s, 2.62 rad/s, 2.24 rad/s for B_d/h=0.0833, 0.167 and 0.333, respectively, which are almost in accordance with those where the dissipation coefficient increases in Fig. 11 (e) and the conversion efficiency in Fig. 11 (c) decreases suddenly occurs. The dissipation coefficient includes the contribution from the energy waste of vortex shedding at the edge of floaters and the energy in the gap for the hybrid system. The previous one is almost the same for different gap width, but the energy in the gap increases with the increasing of the gap width due to the fluid mass increases, resulting in the sudden increase of dissipation coefficient and decrease of conversion efficiency near these resonant frequencies.
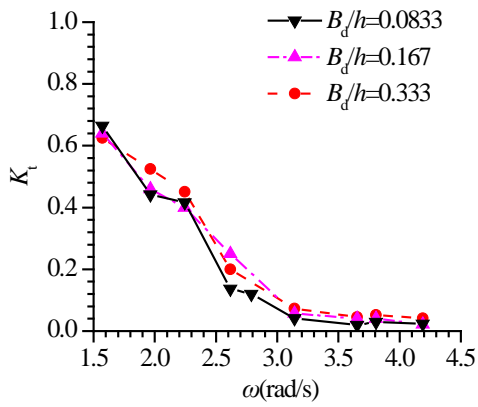
(a) Transmission coefficient

(b) Reflection coefficient

(c) Conversion efficiency

(d) Heave motion

(e) Dissipation coefficient   (f) Wave elevations in the middle of gap
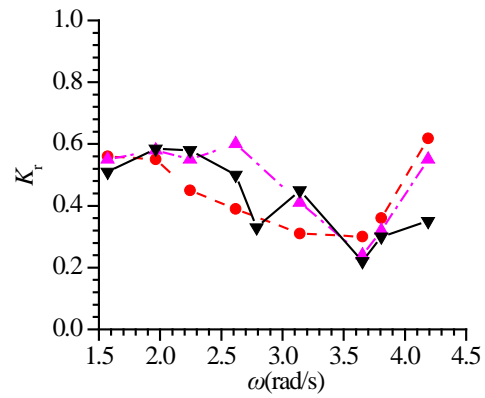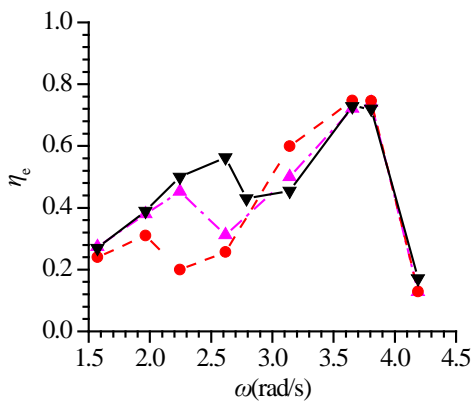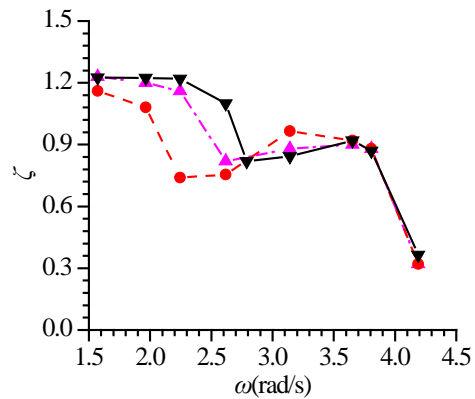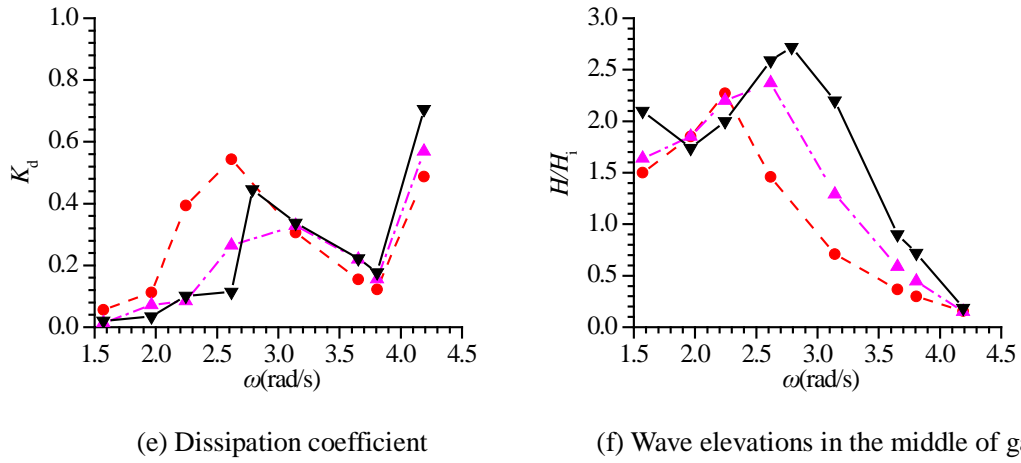
Fig. 11 Variations of ζ, η_e, K_r, K_t, K_d and H/H_i versus ω for different hybrid models with triangular-baffle bottom under the optimal PTO
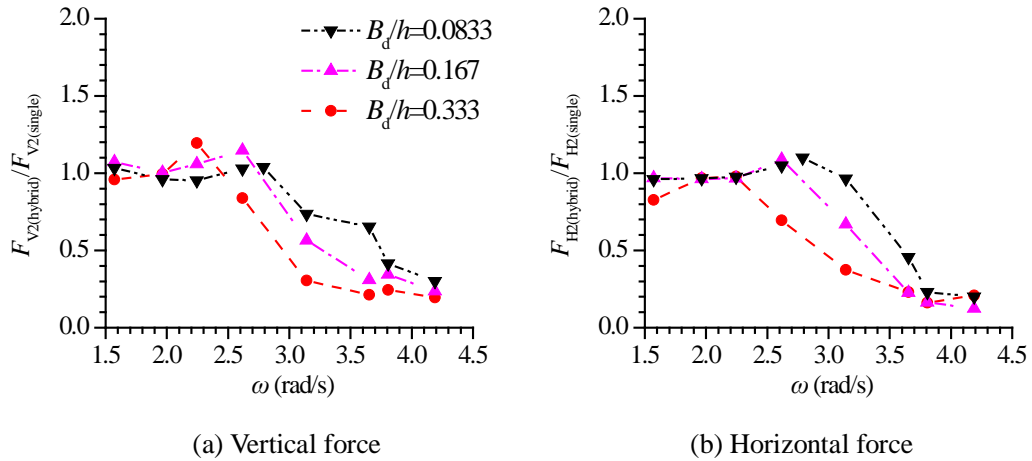
Fig. 12 shows the comparison of the vertical and horizontal forces on the breakwater of the hybrid system with triangular-baffle bottom under the optimal PTO. As with Fig. 10, the horizontal and vertical forces on the breakwater are closely related to the wave elevation in the gap due to much smaller transmitted waves behind the breakwater, especially in the high frequency region. The horizontal and vertical forces are generally reduced due to the front WEC capturing some of the wave energy, except near the wave resonant frequency in the gap. As the gap width increases, the forces decrease because of the smaller wave elevation in the gap.

(a) Vertical force   (b) Horizontal force

Fig. 12 Comparison of the vertical and horizontal forces on the breakwater of hybrid system with triangular-baffle bottom under the optimal PTO

4.3 Effect of WEC draft d_1/h

The hybrid breakwater and triangular-baffle WEC system with three different WEC drafts d_1/h=0.333, 0.267, 0.2 was considered in order to study the effect of the WEC draft d_1/h on the system performance. Fig. 13 shows the variation of transmission coefficient K_t, reflection coefficient K_r, conversion efficiency η_e, dissipation coefficient K_d, heave motion ζ and wave

elevation in the middle of gap H/H_i of the hybrid system against wave frequency for models with different WEC drafts B_1/h under the optimal PTO.

As shown in Fig. 13 (a), the transmission coefficients K_t of the three cases are largely unchanged, as K_t is mainly determined by the breakwater draft. From Fig. 13 (b), it can be seen that the reflection coefficient for the largest WEC draft d_1/h=0.333 is the smallest in the region 2.25 $<\omega<$3.3rad/s, and largest when 3.45$<\omega<$4.65rad/s. As shown in Fig. 13(c), the maximum conversion efficiency η_e and the effective frequency range increase significantly with increasing WEC draft, with the maximum η_e=61.3%, 72.8%, 77.9% respectively. The only changes in heave occur around the peak efficiency point, otherwise largely unchanged, as shown in Fig. 13(d). According to the linear theory, the resonance frequencies are 3.26 rad/s, 3.65 rad/s, and 4.2 rad/s for d_1/h=0.333, 0.267, 0.2, respectively, but the maximum conversion efficiency η_e occurs at 3.65 rad/s. It can be seen from Fig. 13(e) that the dissipation coefficient K_d at ω=3.26 rad/s is larger than that at ω=3.65 rad/s for d_1/h=0.333, due to the wave resonance in the gap in Fig. 13 (f), which results in the peak wave frequency shifting from 3.26 rad/s to 3.65 rad/s for d_1/h=0.333. Similarly, the dissipation coefficient K_d at ω=4.2 rad/s is larger than that at 3.65 rad/s for d_1/h=0.2, due to the strong nonlinearity, which leads to the peak wave frequency shifts from 4.2 rad/s to 3.65 rad/s. There are sudden reductions of conversion efficiency η_e in Fig. 13 (c), and the corresponding wave frequencies are ω=2.62 rad/s, 2.75 rad/s, 3.14 rad/s for d_1/h=0.333, 0.267 and 0.2, respectively. This occurs in conjunction with where the maximum wave elevations in the middle of the gap occurs, as shown in Fig. 13 (f), and the sharp increase of the dissipation in Fig. 13 (e). Wave resonance in the gap causes more energy dissipation and thus the reduction of conversion efficiency η_e. As the WEC draft decreases, the resonance frequency of wave elevation in the gap shifts to higher frequencies, and the peak value decreases, in accordance with previous studies [24].
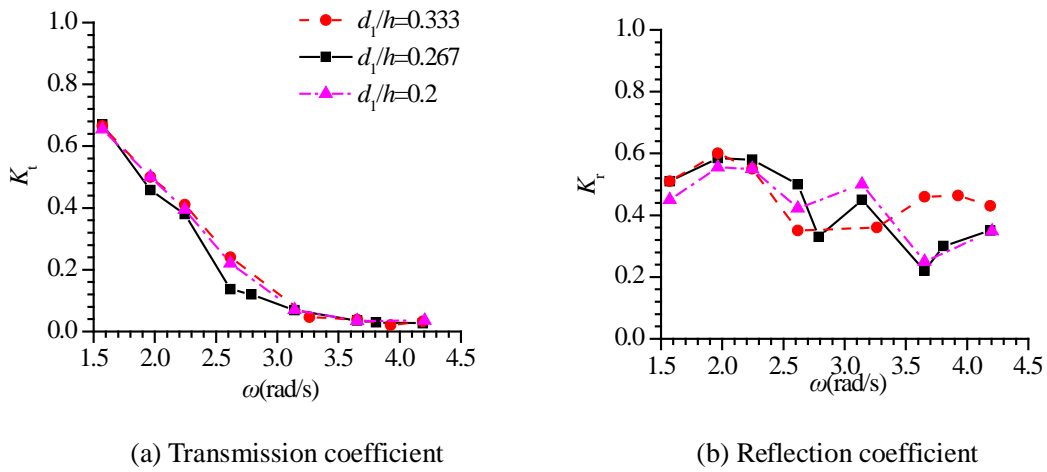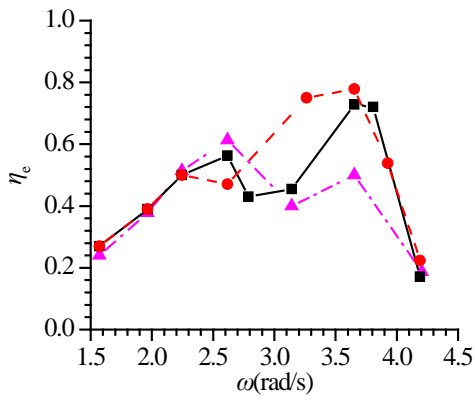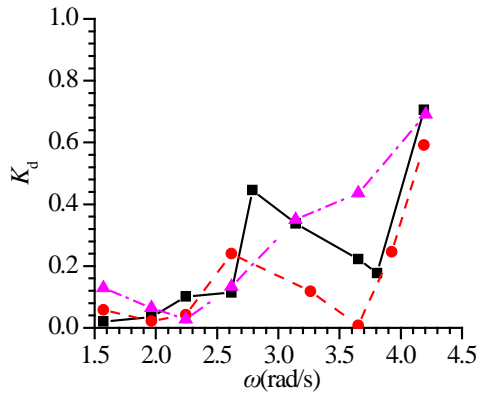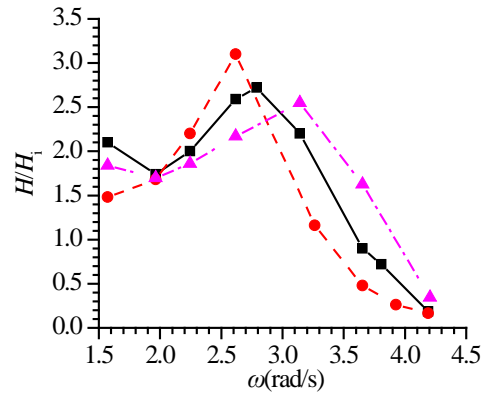

(a) Transmission coefficient   (b) Reflection coefficient

(c) Conversion efficiency
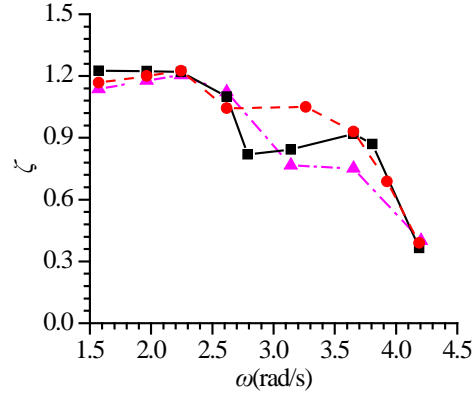
(d) Heave motion

(e) Dissipation coefficient

(f) Wave elevations in the middle of gap

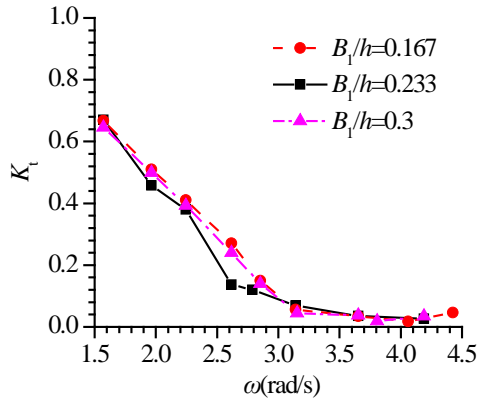Fig. 13 Variations of ζ, η_e, K_r, K_t, K_d and H/H_i versus ω for models with different WEC drafts d_1/h under the optimal PTO

4.4 Effect of WEC width B_1/h

In this section, three different WEC widths of B_1/h=0.167, 0.233, 0.3 were considered to investigate the effect of WEC width B_1/h on the hydrodynamic performance of the hybrid system of the breakwater and the WEC with triangular-baffle bottom. The other parameters were consistent with those in Section 4.1. Fig. 14 shows the variation of transmission coefficient K_t, reflection coefficient K_r, conversion efficiency η_e, heave motion ζ, dissipation coefficient K_d and wave elevation in the middle of gap H/H_i of the hybrid system against wave frequency for models with different WEC widths B_1/h under the optimal PTO.

As shown in Fig. 14(a), the transmission coefficient K_t is largely unaffected by the increase of the WEC width, because the WEC and breakwater drafts, which have the largest influence on K_t are kept constant. Fig. 14(b) shows the reflection coefficient for B_1/h=0.3 is the smallest in low frequencies but the largest in high frequencies. Increasing WEC width leads to increased conversion efficiency η_e for ω<3.15 rad/s, and a decrease in the higher frequency region ω>3.15 rad/s, as

shown in Fig. 14 (c). Fig. 14(f) shows the wave resonance in the WEC-breakwater gap occurs near ω=2.85 rad/s for different WEC widths, demonstrating that WEC width is less important than the distance between two bodies and the draft of the front floater on the resonance frequency of wave elevation in the gap. Conversion efficiency around the gap resonance frequency reduces because of the increased energy dissipation in the gap. The maximum value of η_e is largely unchanged, varying only 4% between the largest and smallest WEC widths. Linear theory predicts that the resonance frequencies are 4.06 rad/s, 3.65 rad/s, and 3.15 rad/s for B_1/h=0.167, 0.233, 0.3, respectively, but the maximum η_e occurs around ω=3.65 rad/s in all cases. This is closely related to the dissipation coefficient K_d shown in Fig. 14 (e). The dissipation coefficient K_d at ω=3.15 rad/s is larger than that at 3.65 rad/s for B_1/h=0.3 due to the wave resonance in the gap in Fig. 14 (f). Similarly, the dissipation coefficient K_d at ω=4.06 rad/s is larger than that at 3.65 rad/s for B_1/h=0.167, due to the strong nonlinearity. The reduction in heave motion with decreasing WEC width in Fig. 14 (d) is due to the corresponding reduction WEC mass. Consequently, the heave motion will be larger for an incident wave of a given size.
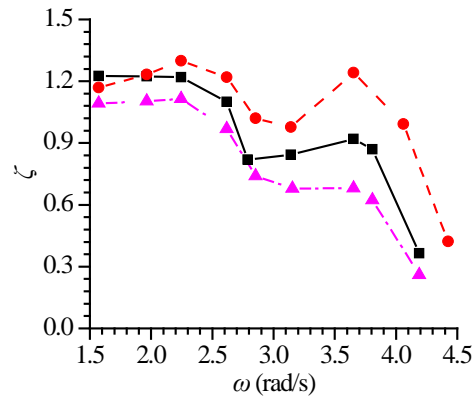

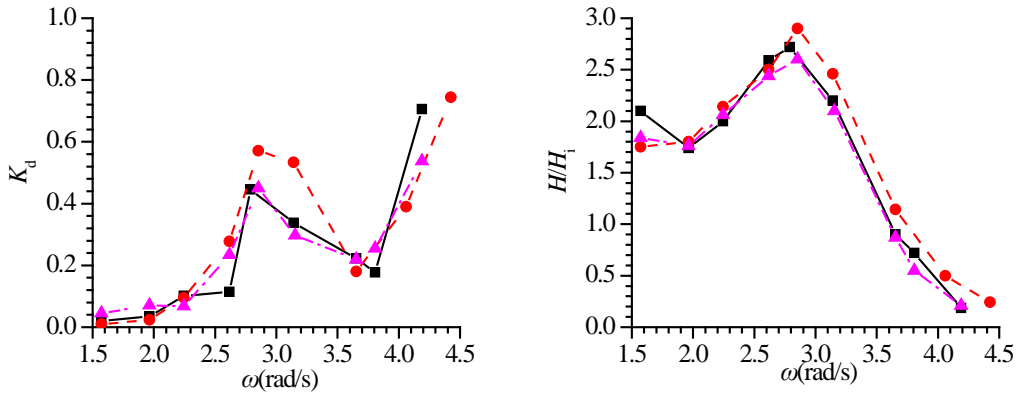(a) Transmission coefficient
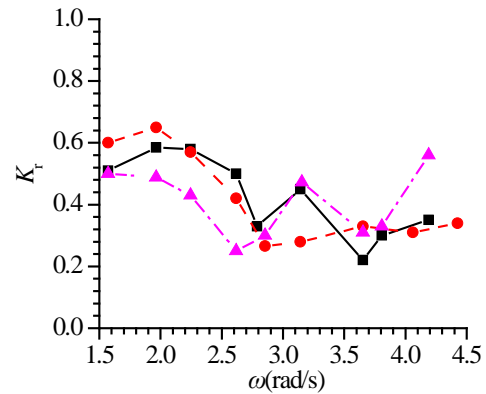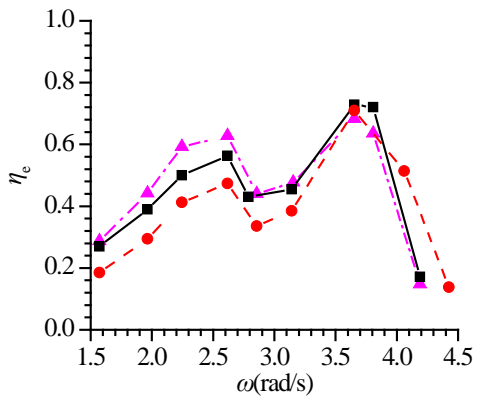
(b) Reflection coefficient

(c) Conversion efficiency

(d) Heave motion

(e) Dissipation coefficient   (f) Wave elevations in the middle of gap

Fig. 14 Variations of ζ, η_e, K_r, K_t, K_d and H/H_i versus ω for hybrid triangular-baffle models with different WEC

widths B_1/h under the optimal PTO

4.5 Effect of incident wave height H_i/h

In linear theory, the transmission coefficient K_t, reflection coefficient K_r, conversion efficiency η_e, heave motion ζ, dissipation coefficient K_d, and wave elevation in the middle of gap H/H_i are expected to be independent of the incident wave height H_i. However, the nonlinearity of wave interaction with floating bodies is closely related to the body shape and the ratio of incident wave height and wave length. The other parameters were consistent with those in Section 4.1. Hybrid system performance for three assumed incident wave heights H_i/h =0.033, 0.1 and 0.167 under the optimal PTO is shown in Fig. 15 and Fig. 16 for the triangular-baffle and square WEC hybrid systems respectively.

Fig. 15(a) and Fig. 16(a) show that there is relatively little difference in K_t for two cases. From Fig. 15(b), it can be seen that the reflection coefficient of the hybrid system with triangular-baffle WEC for incident wave height H_i/h =0.167 is the largest in low frequencies, but for the hybrid system with triangular-baffle WEC, the trend is opposite, as shown in Fig. 16(b). The conversion efficiency η_e in Fig. 15 (c) and Fig. 16 (c) decreases more significantly with the increasing incident wave height, especially at higher wave frequencies, similar to the heave motion, as shown in Fig. 15 (d) and Fig. 16 (d). The more distinct reduction in the conversion efficiency η_e and the heave motion ζ for the hybrid system with triangular-baffle bottom at higher wave frequencies is because of the variation of cross section during heave motion. The nonlinearity becomes stronger as the ratio of relative incident wave height and wave length H_i/λ increases, where the larger incident wave height H_i and the smaller wave length λ at higher frequency leads the ratio to be larger. The maximum reduction ratio of the conversion efficiency η_e reaches 78.5% for the triangular-baffle bottom, and 76.3% for the square bottom both at the highest wave frequency.

The dissipation coefficient K_d in Fig. 15 (e) and Fig. 16 (e) increases as the incident wave height

H_i increases, except ω=3.14 rad/s for the triangular-baffle bottm. The increase is more significant at higher frequency. Consequently, more energy is dissipated as the incident wave height H_i or the wave frequency increases due to stronger nonlinearity. Furthermore, energy dissipation is greater for the square bottom generally, because much stronger vortices develop near the corner of the square bottom than the triangular-baffle bottom during heave motion.

Jiang et al. [23] and Gao et al. [26] found that the wave response in the gap decreased as wave height increased, while the resonant frequency in the gap were nearly the same. When the wave resonances develops in the gap near ω=2.79 rad/s, the dissipation coefficient increases and the conversion efficiency decreases suddenly for the hybrid system with the triangular WEC, as shown in Fig. 15. With increasing wave height, the stronger wave nonlinearity may lead to more energy loss in the gap, so the relative wave response in the gap decreases. The dissipation coefficient includes the contribution to energy losses from vortex shedding at the edge of floaters and the energy in the gap for the hybrid system. Although the energy in the gap decreases, the former increases more significantly due to the stronger nonlinearity, resulting in similar dissipation coefficients, as shown in Fig. 15(e). The above comparisons show as the incident wave height increases, more energy is dissipated, and less energy is transmitted and extracted by the PTO system for both WEC shapes.
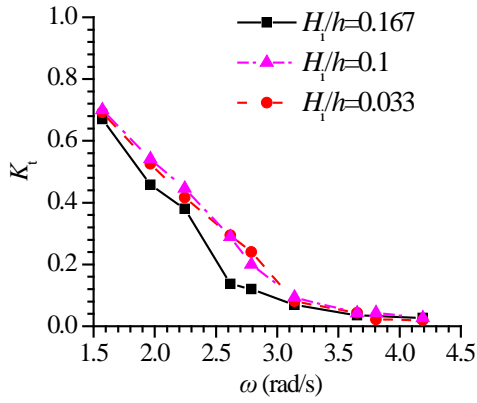
(a) Transmission coefficient
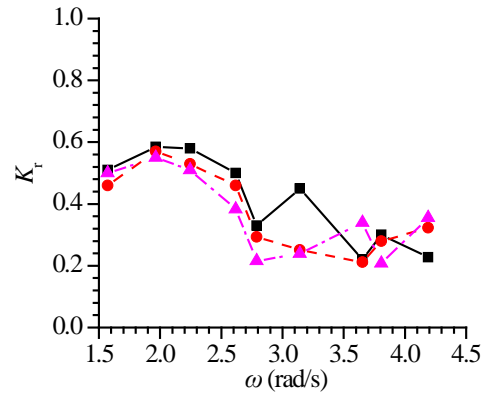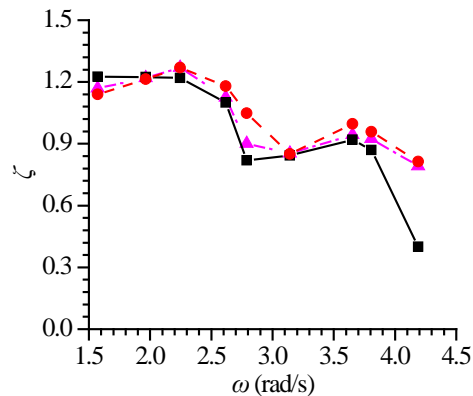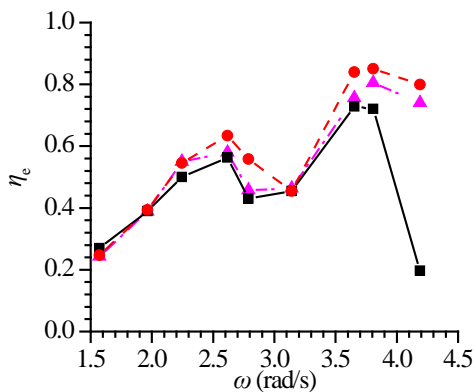
(b) Reflection coefficient

(e) Dissipation coefficient

(f) Wave elevation in the middle of gap

Fig. 15 Variations of K_t, K_r, η_e, ζ, K_d and H/H_i versus ω with different wave heights under the optimal PTO for the

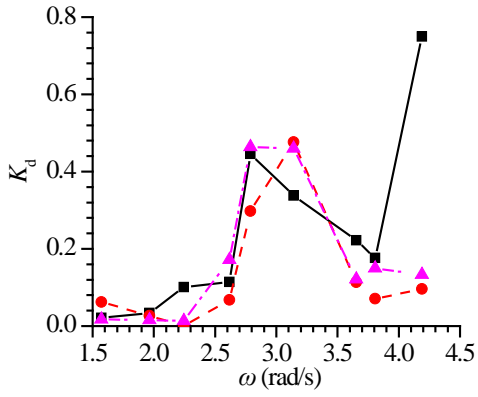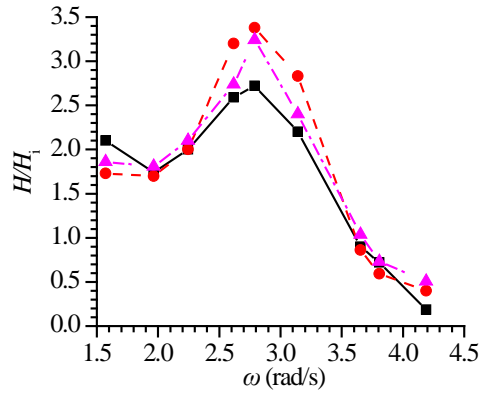hybrid system with triangular-baffle bottom

(a) Transmission coefficient
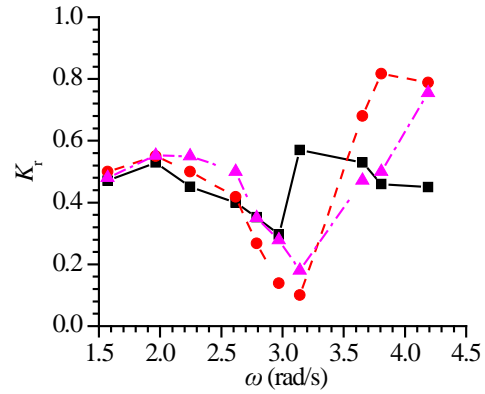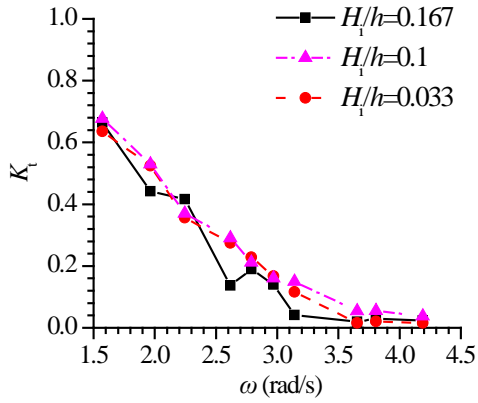
(b) Reflection coefficient

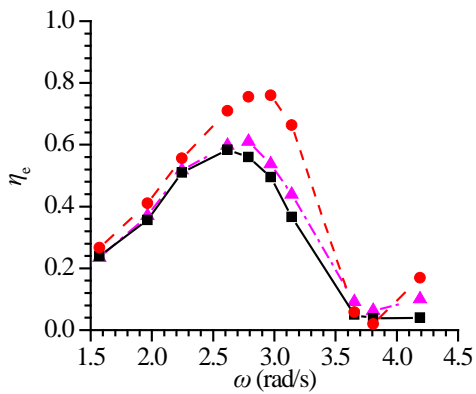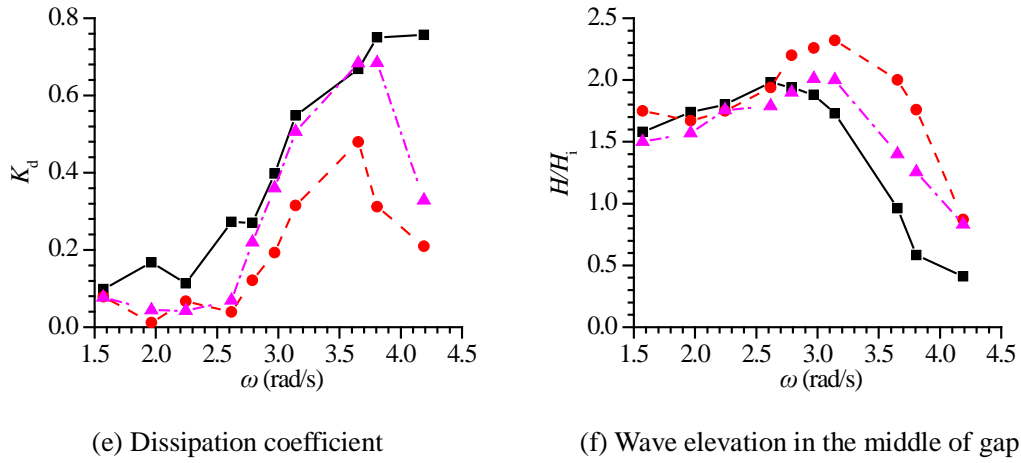(c) Conversion efficiency

(d) Heave motion

26

(e) Dissipation coefficient   (f) Wave elevation in the middle of gap
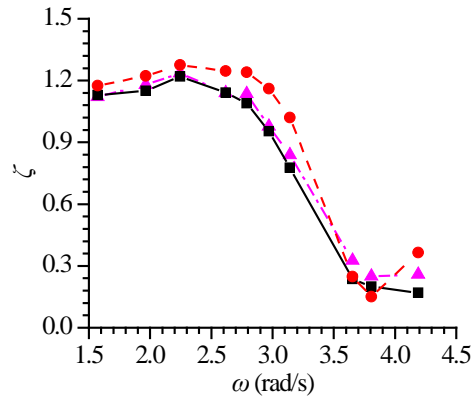
Fig. 16 Variations of K_t, K_r, η_e, ζ, K_d and H/H_i versus ω for different wave heights under the optimal PTO for the hybrid system with square bottom

This study shows that the presence of a breakwater can improve the wave attenuation and wave energy extraction of a WEC at low wave frequencies, and the forces acting on a breakwater can be reduced by a WEC. This means the hybrid WEC-breakwater device has higher performance and longer maintenance cycle in practical engineering applications, which reduces the cost of the wave energy utilization and wave attenuation. Wave resonance in the narrow gap between the WEC and breakwater has an adverse effect on the energy extraction performance of the hybrid system with an asymmetric WEC and increases the forces on the breakwater, which should be avoid in practical designs. The geometrical parameters studied here provide guidance for device optimization.

5. Conclusions

In this paper, the hydrodynamic performance of a dual-floater hybrid system consisting of a floating breakwater and an oscillating-buoy type wave energy converter (WEC) was investigated using Star-CCM+ Computational Fluid Dynamics software, forcusing on the wave energy conversion and attenuation performance of the hybrid system. The following conclusions can be drawn from this study:

(1) The transmission coefficient of the hybrid system is smaller than those of the single WEC and the single breakwater across all wave frequencies, especially compared to the single WEC. The conversion efficiency of the hybrid system increases greatly in the low frequency region for both symmetric and asymmetric bottoms compared with the single WEC.

(2) Compared to the single WEC, wave resonance in the narrow gap between the WEC and the breakwater leads to an increase in the dissipation coefficient and reduction in conversion efficiency of the hybrid system with asymmetric WEC, but leads to a decrease in the dissipation coefficient and the increase in conversion efficiency of the symmetric WEC. The vertical and horizontal forces on the breakwater of the hybrid system are generally reduced. The resonant frequency tends to

increase with decreasing distance between the WEC and breakwater and the WEC draft. The peak wave amplitude in the gap increases with decreasing gap distance and increasing incident wave height. However, the WEC width and incident wave height are less important than the gap width and the WEC draft on the resonance frequency in the gap.

(3) Reducing the distance between the WEC and the breakwater can widen the effective frequency region, but can not change the maximum conversion efficiency η_e. However, the forces on the WEC and the breakwater may be increased at some frequencies, which should be considered.

(4) As the incident wave height increases, the transmission coefficient, the conversion efficiency, the heave motion decrease, and the dissipation coefficient increases for both WEC shapes. The reflection coefficient increases for the triangular-baffle bottom across almost all wave frequencies, while decreases for the square bottom except near $\omega=3.14$rad/s.

The findings of this work can provide valuable guidance for combing wave extraction and costal protection performance to deliver hybrid WEC-breakwater system that achieves cost-sharing, helping make wave energy economically competitive and commercial-scale wave power operations possible.

Acknowledgement

References

[1] Ferro BD. Wave and tidal energy. Refocus 2006;7(3):46-8.

[2] Zhao XL, Ning DZ, Zou QP, Qiao DS, Cai SQ. Hybrid floating breakwater-WEC system: A review. Ocean Eng 2019; 186:106126.

[3] Perez-Collazo C, Greaves D, Iglesias G. Hydrodynamic response of the WEC sub-system of a novel hybrid wind-wave energy converter. Energy Convers and Manage 2018; 171:307-325.

[4] He F, Huang ZH, Law WK. An experimental study of a floating breakwater with asymmetric pneumatic

chambers for wave energy extraction. Appl Energy 2013; 106(11): 222-231

[5] He F, Leng J, Zhao X. An experimental investigation into the wave power extraction of a floating box-type breakwater with dual pneumatic chambers. Appl Ocean Res 2017; 67:21–30.

[6] He F, Zhang HS, Zhao JJ, Zheng SM, Iglesias G. Hydrodynamic performance of a pile-supported OWC breakwater: An analytical study. Appl Ocean Res 2019; 88:326-340.

[7] Xu CH, Huang ZH. A dual-functional wave-power plant for wave-energy extraction and shore protection: A wave-flume study. Appl Energy 2018; 229: 963-976.

[8] Zheng SM, Zhang YL, Iglesias G. Coast/breakwater-integrated OWC: A theoretical model. Marine Struct 2019; 66:121-135.

[9] Giacomo M, Giovanni M, Andrea S, Luca D, Alessandra R, Rocco V, Marco F, Felice A. Modelling and field testing of a breakwater-integrated U-OWC wave energy converter with dielectric elastomer generator. Renew Energy 2020; 146: 628-642.

[10] Han Z, Liu Z, Shi HD. Numerical study on overtopping performance of a multi-level breakwater for wave energy conversion. Ocean Eng 2018; 150:94-101.

[11] Ning DZ, Zhao XL. Hydrodynamic performance of a pile-restrained WEC-type floating breakwater: An experimental study. Renew Energy 2016; 95:531-541.

[12] Zhao XL, Ning DZ, Zhang CW, Kang HG. Hydrodynamic Investigation of an Oscillating Buoy Wave Energy Converter Integrated into a Pile-Restrained Floating Breakwater. Energies 2017; 10:712.

[13] Chen Q, Zang J. On the hydrodynamic performance of a vertical pile-restrained WEC-type floating breakwater. Renew Energy 2018; 146:414-425.

[14] Yeung RW, Wehausen JV, Webster WC. Hydrodynamics of ships and ocean systems-II, lectures notes for course NAOE-241b. Tech.rep, University of California at Berkeley; 1983.

[15] Madhi F, Sinclair ME, Yeung RW. The Berkeley Wedge: an asymmetrical Energy-Capturing floating breakwater of high performance. Marine Syst & Ocean Tech 2014; 9(1):05-16.

[16] Madhi F, Yeung RW. On survivability of asymmetric wave-energy converters in extreme waves. Renew Energy 2018; 119:891–909.

[17] Zhang HM, Zhou BZ, Vogel C, Willden R, Zang J, Zhang L. Hydrodynamic performance of a floating breakwater as an oscillating-buoy type wave energy converter. Appl Energy 2020, 257: 113996.

[18] Ning DZ, Zhao XL, Zhao M, Hann M, Kang HG. Analytical investigation of hydrodynamic performance of a dual pontoon WEC-type breakwater. Appl Ocean Res 2017; 65:102-111.

[19] Zhao XL, Ning DZ. Experimental investigation of breakwater-type WEC composed of both stationary and floating pontoons. Energy 2018; 155:226-233.

[20] Zheng SM, Zhang YL. Analysis for wave power capture capacity of two interconnected floats in regular waves. J. Fluids Struct 2017; 75:158–173.

[21] Reabroy R, Zheng XB, Zhang L, Zang J, Yuan Z, Liu MY, Sun K, Tiaple Y. Hydrodynamic response and power efficiency analysis of heaving wave energy converter integrated with breakwater. Energy Convers Manage 2019; 195:1174-1186.

[22] Li YJ, Zhang CW. Analysis of wave resonance in gap between two heaving barges. Ocean Eng 2016;

17:210-220.

[23] Jiang SC, Bai W, Tang GQ. Numerical simulation of wave resonance in the narrow gap between two non-identical boxes. Ocean Eng 2018; 156:38-60.

[24] Ning DZ, Zhu Y, Zhang CW, Zhao M. Experimental and numerical study on wave response at the gap between two barges of different draufhts. Appl Ocean Res 2018; 77:14-25.

[25] Feng X, Bai W, Chen XB, Qian L, Ma ZH. Numerical investigation of viscous effects on the gap resonance between side-by-side barges. Ocean Eng 2017; 145:44-58.

[26] Gao JL, Zang J, Chen LF, Chen Q, Ding HY, Liu YY. On hydrodynamic characteristics of gap resonance between two fixed bodies in close proximity. Ocean Eng 2019; 173:28-44.

[27] Bilandi RN, Jamei S, Roshan F. Numerical simulation of vertical water impact of asymmetric wedges by using a finite volume method combined with a volume-of-fluid technique. Ocean Eng 2018; 160:119-131.

[28] Kim JW, O'Sullivan J, Read A. Ringing Analysis on a Vertical Cylinder by Euler Overlay Method. OMAE 2012-84091.

[29] Choi J, Sung BY. Numerical simulations using momentum source wave-maker applied to RANS equation model. Coastal Eng 2009; 56(10):1043-1060.

[30] Fenton JD. A fifth-order stokes theory for steady waves. J Waterw Port, Coast Ocean Eng 1985; 111(2): 216-234.

[31] Fábio MMM, António MGL, Almerindo DF. Numerical simulation of regular waves: Optimization of a numerical wave tank. Ocean Eng 2018; 170:89–99

[32] Völkner S, Brunswig J, Rung T. Analysis of non-conservative interpolation techniques in overset grid finite-volume methods. Comput Fluids 2017; 148:39–55.

[33] Sun SY, Sun SL, Wu GX. Fully nonlinear time domain analysis for Hydrodynamic performance of an oscillating wave surge converter. China Ocean Eng 2018; 32(5):582-592.

[34] Zhou BZ, Ning DZ, Teng B, Bai W. Numerical investigation of wave radiation by a vertical cylinder using a fully nonlinear HOBEM. Ocean Eng 2013; 70:1-13.

[35] Zhou BZ, Wu L, Xu GD. Resonance of the roll motion of a two dimensional barge induced by triple frequency wave force. Ocean Eng 2017; 134:13-23.

[36] Budar K, Falnes J. A resonant point absorber of ocean-wave power. Nature 1975; 256 (5517):478-479.